Volume 18, Number 1, 2025. pp. 1-9

Jordan Journal of Physics

ARTICLE

Optimizing Optoelectronic, Antimicrobial Activity and Electrical Properties of Composite ZnO/ZnS with Fe Doped Nanocomposite towards Applications in Water Treatment

J. Barman[a], **M. Bhattacharjee**[b] and **D. J. Haloi**[c]

[a] *Department of Physics, ADP College, Nagaon, Assam-782002, India.*
[b] *Department of Chemistry, Bodoland University, Kokrajhar, Assam-783370, India.*
[c] *Department of Applied Science, Tezpur University, Assam-784028, India.*

Doi: **https://doi.org/10.47011/18.1.1**

Received on: 20/03/2023; *Accepted on: 21/12/2023*

Abstract: Composite ZnO and ZnS nanostructured with Fe doping thin films, exhibiting high antimicrobial activity, have been synthesized by chemical route. The optimized parameters, including composition ratio, doping concentration, temperature, UV exposure, and thickness of the composite ZnO and ZnS films, have been optimized in thin-film form. The synthesized samples were identified and analyzed by XRD, HR-SEM, EDX, and HRTEM. The band gap was estimated from absorption spectra, and the Stokes shift energy was calculated from emission and absorption spectra. The conductivity of the samples increased with higher Fe content and it depended on the composite ratio of ZnO and ZnS. Antimicrobial properties were studied using four bacterial strains, revealing that a concentration of 3.5 wt% was the optimal value for the most efficient activity.

Keywords: Nanocrystalline thin films, ZnO/ZnS, Antimicrobial, XRD, Optical, Electrical properties.

Introduction

Composite materials like ZnO and ZnS have tremendous importance in frontier research due to their extraordinary physical, chemical, biological, and electrical properties. These semiconductor materials can be used as eco material of choice for key applications in water treatment. The properties of composite materials depend on the synthesis method, including starting parameters.

The promising applications of nanocomposites have been widely explored across various fields. The nanocomposite materials exhibit significant potential in optoelectronics as well as electrical conductivity. When these compound materials are doped with suitable elements, they acquire enhanced properties, that can be applied in various fields, including biomedical applications [1-3].

Among the various nanocomposite materials, ZnO/ZnS is an attractive candidate due to its distinguished performance in conductivity and high performance in antimicrobial activity. When ZnO/ZnS composite is doped with Fe, its application range becomes wider, making it highly suitable for water treatment due to the dependence property of conductivity and antimicrobial properties [4-7].

The existence of bacteria in drinking water is a major issue in most of the country. In this context, composite ZnO/ZnS doped with Fe exhibits attractive antibacterial properties. These composite nanomaterials have a large surface-to-volume ratio. From the literature, it was observed that the toxicity of ZnO/ZnS has minimal effect on living cells [8-11]. Various mechanisms in ZnO/ZnS nanocomposites

Corresponding Author: J. Barman **Email**: jayantabarman2006@gmail.com

contribute to their antibacterial activity due to the ion exchange with cell membranes [12-18]. ZnO/ZnS has ferromagnetic properties at room temperature. When doped with Fe, it becomes an attractive candidate for application in antimicrobial activity [19]. Doping with Fe alters the conductivity and enhances antimicrobial effects. The present work focuses on the fabrication process to determine the optimal parameters of composite ratio, doping concentration, photon-induced time, and reaction rate for high efficiency in antimicrobial activity for the reduction of environmental burden. The prepared samples were analyzed with XRD, UV-visible spectrometer, EDX, SEM, PL, and electrical measurements.

Experimental

Sample Preparation and Characterization Techniques

The composite nanoparticles were synthesized by the chemical method at different wt% of the doping material. The doping concentration ranged from 0.5 to 4.0 wt%. The key chemicals were mainly sourced from Merck, India. All the materials used were of analytic grade and were used without further purification. ZnS and NaOH with Na_2S. The materials used were of analytical grade. The required chemicals were dissolved in double-distilled water and stirred for 12 hours, both under vacuum and non-vacuum conditions, until the solution became clear and transparent. After preparation, the doping material Fe was added in different wt% concentrations, poured into a silica crucible, and subjected to microwave exposure. After 24 hours, the prepared samples were cast onto a glass substrate to form thin films and dried in a vacuum environment for 6 hours. The final samples were washed multiple times with alcohol to remove any remaining ions and then dried in a hot air oven at 70°C for 2 h.

The synthesized Fe-doped ZnO/ZnS nanocomposite was characterized using UV- VIS spectrophotometry (Systronics), XRD (Phillips X'Pert Pro Powder X-ray Diffractometer), SEM (JSM-6360, JEOL), TEM (Model: JEM-100 CX II), and photoluminescence studies.

Test for Antibacterial Activity

Escherichia coli (MTCC 739), *Klebsiella pneumonia* (MTCC 432), *Pseudomonas aeruginosa* (MTCC-424), and *Staphylococcus aureus* (MTCC-740) were used for antibacterial screening. The microbial cultures were purchased from the "Microbial Type Culture Collection and Gene Bank" (MTCC), Chandigarh, India. The bacterial cultures were maintained on nutrient agar slants and were stored at -4°C. The solutions were made at concentrations of 10, 30, and 50 μg/ml by adding 100 mg of each sample in 1 ml of DMSO with proper dilution.

The antimicrobial activity of Fe-doped and undoped ZnO/ZnS composites was analyzed using the well-diffusion method [20-22]. Nutrient agar plates were used, and 2.5 mL of bacterial inoculum was spread evenly over each plate. Standard antibiotics (Tetracycline) were used as reference antibacterial agents for both gram-negative and gram-positive bacteria. The ZnO/ZnS composites were loaded onto the agar plates and incubated at 37°C for 24 hours. The inhibition zone diameters were measured using a traveling microscope. Antimicrobial activity was assessed for different wt% doping concentrations and ZnO/ZnS composite ratios.

Results and Discussions

Structural Analysis by XRD

Figure 1 shows the composite ZnO/ZnS at different composite ratios and different doping concentrations. The diffraction pattern in the XRD peaks was identified at 2θ = 31.730°, 47.380°, and 51.220°, corresponding to (100), (002), and (101) planes, respectively, for a ZnO/ZnS ratio of 3:5 and a doping concentration of 3.5 wt%.

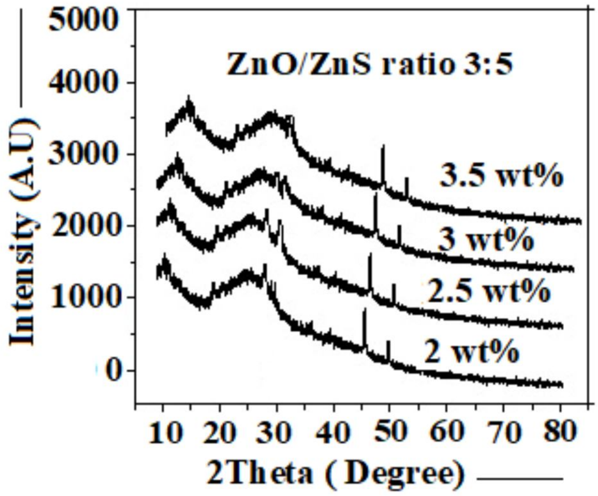

FIG. 1. XRD patterns of the ZnO/ZnS composite at 3:5 ratio for various doping concentrations.

The diffraction peaks are in good agreement with the hexagonal wurtzite-type structure (space group P63mc). With an increase in doping concentration from 2 wt% to 3.5 wt% at the ZnO/ZnS ratio 3:5, the peaks are slightly diffracted to a higher diffraction angle and broadened, indicating a decrease in crystallinity. The optimum doping concentration is found at 3.5 wt%, as evidenced by the most significant structural refinement. Additionally, Fe peaks are observed at $2\theta = 46°$.

The XRD spectrum shows a mixed-phase structure, which explains the multiple peaks observed in the absorption spectra. The replacement of ZnO/ZnS lattice ions by Fe^{2+} ions is further confirmed by TEM. The average crystallite size was calculated using the Debye-Scherrer equation by considering full-width at the half-maximum (FWHM) of the first intense peak (100) [23, 24].

$$D_{hkl} = F\lambda/M \; Cos\,\theta \tag{1}$$

In Eq. (1), D represents the average crystallite size, θ the Bragg angle, and M the FWHM. The value of F is 0.89 for spherical shape and shape (confirmed by HRTEM). The crystallite size was found to be in the range of 8-14 nm for all samples. Again, it is observed that when the doping concentration increases from 2.0 wt% to 3.5 wt%, the crystallite size decreases. However, for doping levels beyond 3.5 wt%, the crystallite size increases due to rapid nucleation growth, suggesting that 3.5 wt% is the optimal doping concentration [25].

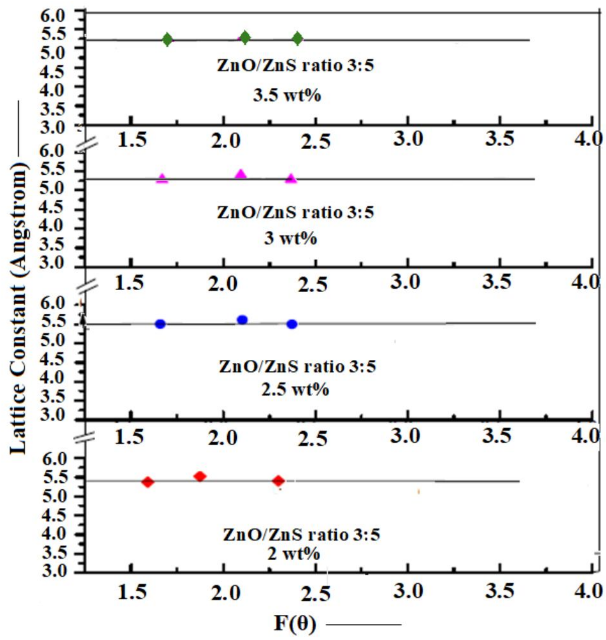

FIG. 2. Nelson–Riley plot of ZnO/ZnS nanocomposite at a 3:5 under different doping concentrations.

Rietveld refinement (RR) analysis was used to characterize in detail the crystalline structure. The lattice parameter increased with an increase of doping concentration beyond 3.5 wt%, clearly indicating that Fe^{2+} ions substitute Zn^{2+} ions in the composite material [26]. The lattice constant was calculated using the Nelson–Riley plot to eliminate strain effects, yielding an average value of 5.4012 Å. Figure 2 shows the Nelson–Riley plot.

From the RR analysis, the values of a and c were calculated, which allowed us to estimate the nearest Zn–O bond length along the c-direction [27].

$$L = \sqrt{\frac{a^2}{3} + \left(\frac{1}{2} - u\right)^2 c^2} ,$$

where a and c represent the lattice parameters, u is the internal parameter, and L is the bond length. The value of c/a was 1.603, which is in good agreement with the hexagonal close-packed structure [27].

TEM Result Analysis

The particle distribution was analyzed by TEM. It was observed that particles were uniformly distributed. Figure 3 represents the optimum condition ZnO/ZnS ratio of 3:5 with 3.5 wt% Fe doping. The average particle diameter was 40 nm, which differs from the values obtained via XRD and optical modeling because XRD gives the average grain size.

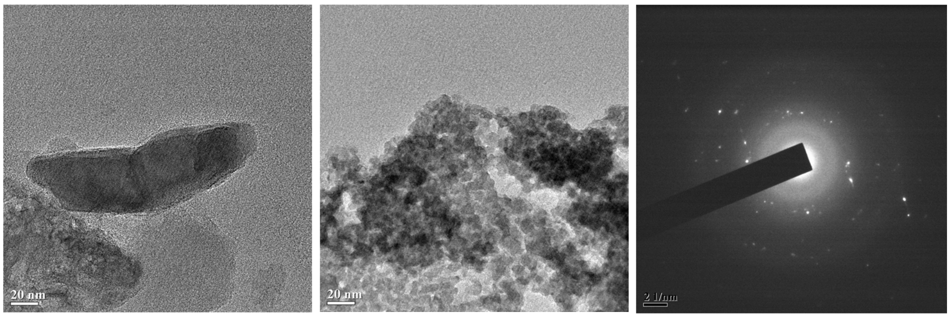

(a) (b) (c)

FIG. 3. TEM micrographs of (a) ZnO/ZnS at a 3:5 ratio, (b) ZnO/ZnS at a 3:5 ratio with Fe doping, and (c) SAED pattern of Fe-doped ZnO/ZnS composite.

TEM EDX Analysis

Elemental analysis was performed through energy dispersive X-ray attached to the TEM. EDX were captured from regions where particles were uniformly distributed, confirming the presence of Zn, S, and Fe. Some silicon peaks were also observed, likely originating from the glass substrate. Multiple regions were analyzed, revealing that Fe-doped areas exhibited larger particle sizes due to the doping concentration. Data analysis indicated that the 3.5 wt% Fe-doped sample contained the highest percentages of Zn, S, and Fe.

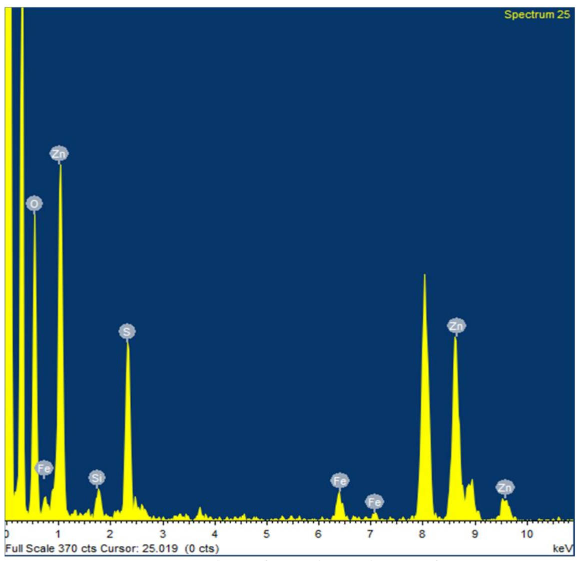

FIG. 4. EDX results of Fe-doped ZnO/ZnS at 3:5.

SEM Analysis

The morphology of the samples was analyzed using an SEM available at NEHU (JSM-6360, JEOL). The SEM analysis confirms that doped samples have larger grain sizes, ranging from 22 to 40 nm. Some samples exhibited a hexagonal shape at a doping concentration of 3.5 wt%. Figure 5(a) shows the undoped ZnO/ZnS nanocomposite at a 3:5 ratio, while Figure 5(b) shows the ZnO/ZnS nanocomposite doped with 3.5 wt% Fe, exhibiting a hexagonal shape that is in good agreement with the XRD pattern. Doping leads to an increase in grain size compared to the undoped samples.

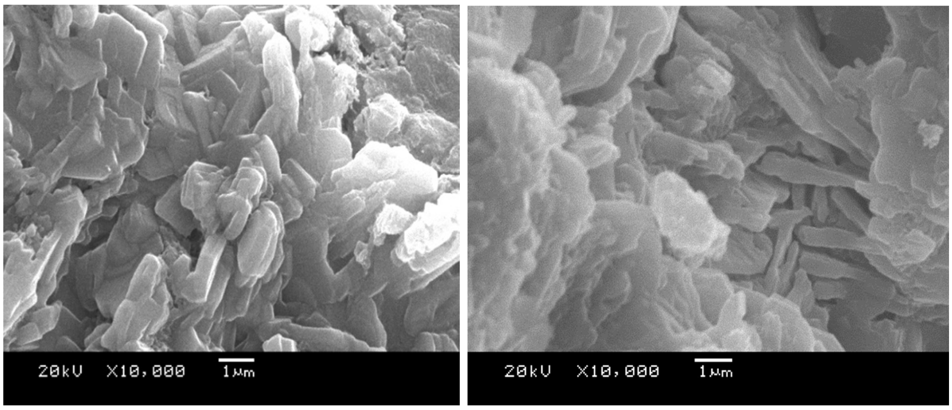

(a) (b)

FIG. 5. SEM images of the nanocomposite: (a) ZnO/ZnS at 3:5 and (b) ZnO/ZnS at 3:5 with 3.5 wt% Fe.

Photoluminescence Studies

Figure 6 shows the PL spectrum of Fe^{2+}-doped ZnO/ZnS composite at 3:5 for different doping concentrations at room temperature. The excitation wavelength is 200 nm. The effect of doping with Fe^{2+} ions on the photoluminescence activity of ZnO/ZnS crystals is evident. The PL spectrum shows five characteristic peaks in all samples at different doping concentrations. wo broad peaks are observed in the ranges of 400 nm and 536 nm. It is noted that as the doping concentration increases, the position of the peaks shifts, indicating a size effect. The doping concentration alters the lattice structure, affecting the Zn^{2+}, S^{2-}, and neighboring OH^{-} ions. The broad peaks may arise due to trap states [28-30].

A blue emission peak is observed in all samples around 425 nm, attributed to Zn vacancies [31]. Low-intensity peaks are observed in the range of 480–570 nm due to sulfur vacancies. A sharp peak is observed at 627 nm, corresponding to the mismatch of Fe^{2+} ions. From the absorbance and emission peaks, the positive Stokes shift energy is calculated, revealing that the Stokes shift energy is larger at lower doping concentrations, which suggests stronger coupling to lattice phonons [32].

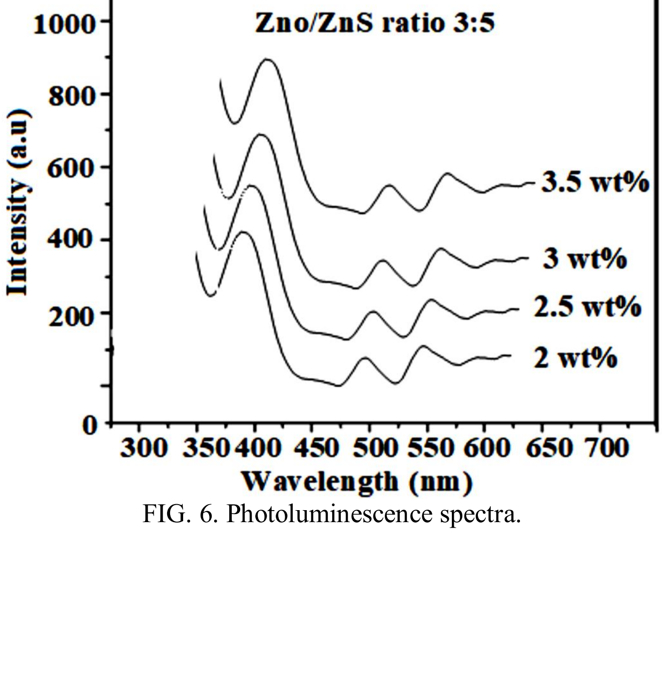

FIG. 6. Photoluminescence spectra.

UV Spectrometric Analysis

The UV-Vis spectrum was analyzed in the range of 300 to 800 nm for all samples. It was found that the absorption shows a blue shift, as shown in Fig. 7. The blue shift energy was calculated using the Tauc plot and was observed to change with varying doping concentrations. Table 1 shows the blue shift energy for different doping concentrations. The blue shift energy depends on both the composite ratio and the doping concentration. It increases up to 4.1 eV with increasing doping concentration, then decreases. The ZnO/ZnS ratio of 3:5 with 3.5 wt% doping concentration is found to be the maximum tunable condition. The decrease in particle size leads to a shift in the blue shift energy, which results in quantum confinement and an increase in the band gap.

The composite ZnO/ZnS shows the best fit for a direct band gap. From Fig. 8, the band gap range is 3.8–4.1 eV, which is an important parameter related to electrical conductivity. Table 1 shows the variation of the band gap with different doping concentrations [32-37].

.

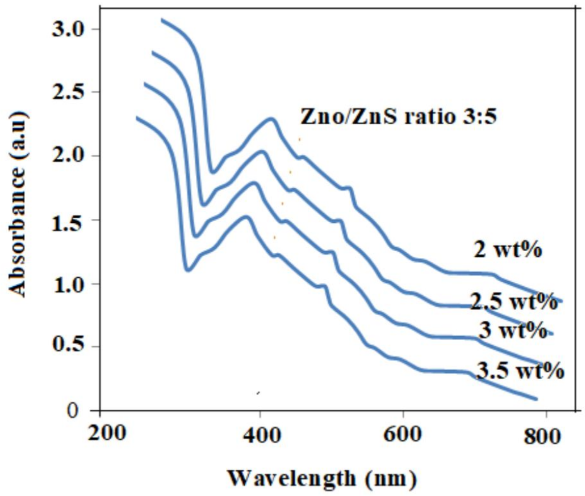

FIG. 7. UV-visible absorption of Fe-doped ZnO/ZnS nanocomposite with a 3:5 ratio.

TABLE 1. Blue shift energy and band gap energy with particle size at different Fe doping concentrations.

Sample No.	Composite Ratio of ZnO and ZnS	Fe Doping Concentration	Energy Band Gap [eV]	Blue Shift Energy [eV]	Particle radius [nm]
A	3:5	2 wt%	3.83	0.16	6.3
B	3:5	2.5 wt%	3.85	0.21	5.9
C	3:5	3 wt%	3.95	0.36	5.2
D	3:5	3.5 wt%	4.03	0.39	4.8

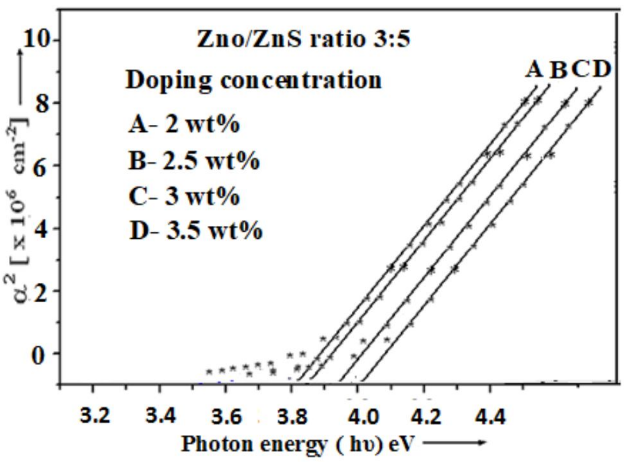

FIG. 8. Tauc plot of composite ZnO /CdS (3:5) at different doping concentrations (2.0 wt% to 3.5 wt%).

The particle radius (r) was calculated using the effective mass approximation method (EMA) with the calculated band gap energy:

$$E_{gn} = [E_{gb}^2 + 2\hbar^2 E_{gb} (\pi/R)^2/m^*], \quad (2)$$

where E_{gb} is the average bulk band gap of ZnO and ZnS, E_{gn} is the calculated band gap energy, and m* is the effective mass of the specimen. The average particle radius is in the range of 4-7 nm.

Antimicrobial Assay

Antibacterial activity was studied for doped and undoped Fe at different wt% with varying composite ratios of ZnO/ZnS against four pathogenic bacteria species: *E. coli*, *B. subtilis*, *K. pneumonia*, and *S. aureus*. Tetracycline (1 mg/mL) was used as a control antibacterial agent. The maximum zone of inhibition was found with 3.5 wt% Fe-doped ZnO/ZnS composite at a 3:5 ratio, as shown in Table 2. It was observed that when the doping concentration was too high, the antimicrobial efficiency decreased. The optimum doping concentration was found to be 3.5 wt%.

The antibacterial activity was determined in vitro by measuring the zone of inhibition (in mm) for samples at different concentrations. As indicated in Table 2, the maximum zone of inhibition was observed for the 3.5 wt% Fe-doped ZnO/ZnS composite at a 3:5 ratio. When the doping concentration was increased beyond this optimal level, the antimicrobial efficiency decreased due to an increase in crystallite size and changes in ionic radius related to the composite ratio.

ZnO-ZnS ratio and Doping concentration	Antimicrobial assay with	Zone inhibition (diameter in nm)	Antimicrobial assay with	Zone inhibition (diameter in nm)
3:5 and 3.5 wt%	S. aureus 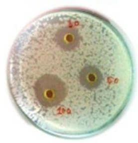	19 nm	B.subtilis 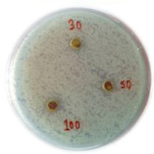	16 nm
3:5 and 3.5 wt%	K. pneumoniae 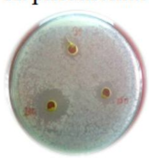	17 nm	E. coli 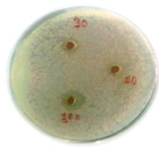	9 nm

FIG. 9. Zone inhibition of ZnO-ZnS at a 3:5 ratio and 3.5 wt% doping concentration against four bacterial cultures.

TABLE 2. Zone inhibition of ZnO-ZnS at a 3:5 ratio of Fe-doped ZnO/ZnS nanocomposite with standard bacterial strains.

Bacteria	Diameter of zone inhibition [nm] ZnO/ZnS nanocomposite at 3:5 at 3.5 wt% Fe Doping			Tetracyclin [1 mg/mL]
	10 μL	30 μL	50 μL	
E. coli	7±0.14	18±0.11	24±0.13	35±0.08
B. subtilis	6±0.11	16±0.16	21±0.15	32±0.09
P. aeruginosa	5±0.15	12±0.14	21±0.11	31±0.09
S. aureus	7±0.11	17±0.08	23±0.11	34±0.11

Electrical Study

The electrical resistivity of Fe-doped nanocomposite ZnO/ZnS thin films was studied using the D.C. two-point probe method. The resistivity of the samples was calculated using the following relation:

$$\boldsymbol{\rho = \rho_0 \, exp(E_a/kT)}, \quad (3)$$

where ρ represents resistivity at temperature T, ρ0 is a constant, and k is the Boltzmann constant. Figure 10 shows that the resistivity decreases as the temperature increases. As the doping concentration increases from 2.0 wt% to 3.5

wt%, conductivity increases, but at higher doping concentrations, conductivity decreases again [38]. Doping creates traps within the crystal, which may decrease the conductivity of the samples.

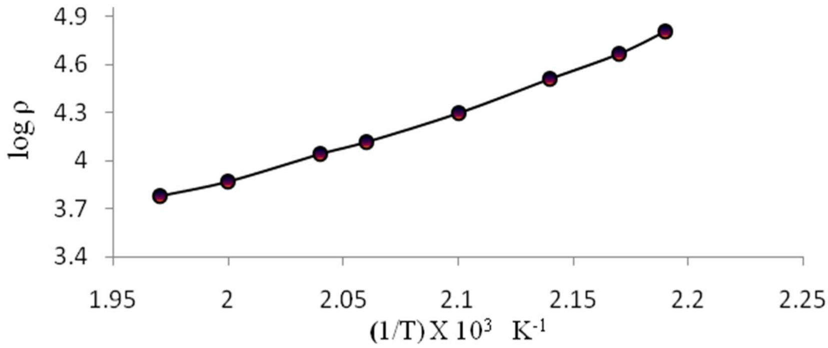

FIG. 10. Variation of log ρ with 1/T for as-deposited Fe-doped ZnO/ZnS at 3.5 wt%.

Conclusion

Composite ZnO and ZnS nanostructured thin films with Fe doping, exhibiting high antimicrobial activity, were synthesized by the chemical route. The optimized parameters, including composition ratio, doping concentration, temperature, and thickness of the film, were optimized in thin film form. Absorption spectra provided the optimum band gap energy, which was found to be in the range of 3.8-4.1 eV. The nanocomposite ZnO/ZnS at 3:5 with 3.5 wt% demonstrated the highest efficiency in all analyses, with a Stokes shift energy of 3.64 eV.

Conductivity increased with higher Fe doping and depended on the composite ratio. The highest antimicrobial activity was observed in the ZnO/ZnS composite with a 3:5 ratio and 3.5 wt% Fe doping concentration. Additionally, at 3.5 wt% Fe doping, electrical conductivity reached its maximum, providing a better understanding of the relationship between particle size, antimicrobial activity, and band gap energy, which increased under these conditions. Energy-dispersive X-ray (EDX) analysis confirmed the presence of Fe, S, Zn, and O in the sample.

Acknowledgments

This work is part of the activities of Biotech Hub and Star College. The authors acknowledge the Department of Biotechnology, Government of India, for financial support.

References

[1] Irimpan L., Nampoori V.P.N., and Radhakrishnan P., J. Appl. Phys., 103 (2008) 1.

[2] Nayak J., Sahu S.N., Kasuya J., and Nozaki S., Appl. Surf. Sci., 254 (2008) 7215.

[3] Sadoun, B., Mouetsi, S., Hocini, A., and Derdour, R., Jordan J. Phys., 16 (2023) 105.

[4] Manoj Kumar, M., Nandi, M., and Pakshirajan, K., J. Environ. Manag., 278 (2021) 111555.

[5] Rao, G.T., Babu, B., Stella, R.J., Manjari, V.P., Reddy, C.V., Jaesool, S., and Ravikumar, R.V.S.S.N, J. Mol. Struct., 1081 (2015) 254.

[6] Liu, J., Zhu, K., Sheng, B., Li, Z., Tai, G., Qiu, J., Wang, J., Chen, J., You, Y., Gu, Q., and Liu, P., J. Alloy. Compd., 618 (2015) 67.

[7] Jana, T.K., Pal, A., and Chatterjee, K., J. Alloy Compd., 583 (2014) 510.

[8] Brayner, R., Ferrari-Iliou, R., Brivois, N., Djediat, S., Benedetti, M.F., and Fievet, F., Nano Lett., 6 (2006) 866.

[9] Thill, A., Zeyons, O., Spalla, O., Chauvat, F., Rose, J., Auffan, M., and Flank, A.M., Environ. Sci. Technol., 40 (2006) 6151.

[10] Reddy, K.M., Feris, K., Bell, J., Wingett, D.G., Hanley, C., and Punnoose, A., Appl. Phys. Lett., 90 (2007) 2139021.

[11] Zhang, L.L., Jiang, Y.H., Ding, Y.L., Povey, M., and York, D., J. Nanopart. Res., 9 (2007) 479.

[12] Kajbafvala, A., Ghorbani, H., Paravar, A., Samberg, J.P., Kajbafvala, E., and

Sadrnezhaad, S.K., Superlattices Microstruct., 52 (2012) 512.

[13] Tarwal, N.L., Devan, R.S., Ma, Y.R., Patil, R.S., Karanjkar, M.M., and Patil, P.S., Electrochim. Acta, 72 (2012) 32.

[14] Yang, W.F., Wu, Z.Y., Liu, Z.G., and Kong, L.M., Appl. Surf. Sci., 256 (2010) 7591.

[15] Luo, L.J., Tao, W., Hu, X.Y., Xiao, T., Heng, B.J., Huang, W., Wang, H., Han, H.W., Jiang, Q.K., Wang, J.B., and Tang, Y.W., J. Power Sources, 196 (2011) 10518.

[16] Pawar, B.N., Cai, G., Hama, D., Mane, R.S., Ganesh, T., Ghule, A., Sharma, R., Jadhava, K.D., and Han, S.H., Sol. Energy Mater. Sol. Cells, 93 (2009) 524.

[17] Park, Y.C., Kong, E.H., Chang, Y.J., Kum, B.G., and Jang, H.M., Electrochim. Acta, 56 (2011) 7371.

[18] Chen, Y., Tao, Q., Fu, W., Yang, H., Zhou, X., Zhang, Y., Su, S., Wang, P., and Li, M., Electrochim. Acta, 118 (2014) 176.

[19] Hsu, S.H., Hung, S.F., and Chien, S.H., J. Power Sources, 233 (2013) 236.

[20] Zhang, C., Huang, Z., Liao, X., Yin, G., and Gu, J., J. Coat. Technol. Res., 9 (2012) 621.

[21] Gummuluri, S., Kavalipurapu, V.T., and Kaligotla, A.V., Braz. Dent. Sci., 22 (2019) 365.

[22] Adeyemi, A.I., Vincent, O.I., and Olujenyo, O.M., Asian J. Med. Biol. Res., 4 (2018) 7.

[23] Ahmed, F., Kumar, S., Arshi, N., Anwar, M.S., Koo, B.H., and Lee, C.G., Microelectron. Eng., 89 (2012) 1290.

[24] Ansari, S.A., Nisar, A., Fatma, B., Khan, W., and Naqvi, A.H., Mater. Sci. Eng. B, 177 (2012) 428.

[25] Mohapatra, J., Misra, D.K., Perumal, A., Medicherla, V.R.R., Phase, D.M., and Singh, S.K., Mater. Res. Bull., 47 (2012) 1417.

[26] Lemine, O.M., Bououdina, M., Sajieddine, M., Saie, A.M.A., Shafi, M., Khatab, A., Alhilali, M.A., and Henini, M., Physica B, 406 (2011) 1989.

[27] Barman, J., Sultana, F., and Banik, B., Romanian J. Biophysics, 31 (2021) 165.

[28] Liu, S.M., Liu, F.Q., Guo, H.Q., Zhang, Z.H., and Wang, Z.G., Solid State Commun., 115 (2000) 615.

[29] Reddy, A.J., Kokila, M.K., Nagabhushana, H., Rao, J.L., Nagabhushana, M., Shiv-akumara, C., and Chakradhar, R.P.S., Spectrochim. Acta A, 79 (2011) 476.

[30] Wu, D., Huang, Z., Yin, G., Yao, Y., Liao, X., Han, D., Huang, X., and Gu, J., Cryst. Eng. Comm., 12 (2010) 192.

[31] Zeng, H., Cai, W., Hu, J., Duan, G., Liu, P., and Li, Y., Appl. Phys. Lett., 88 (2006) 1.

[32] Misra, M., Kapur, P., Ghanshyam, C., and Singla, M.L., J. Mater. Sci. Mater. Electron., 24 (2013) 3800.

[33] Mollaa, A.R., Chakradhar, R.P.S., Kesavulu, C.R., Rao, J.L., and Biswas, S.K., J. Alloy. Compd., 512 (2012) 105.

[34] Burstin, E., Phys. Rev., 93 (1954) 632.

[35] Moss, T.S., Proc. Phys. Soc. Sect. B, 67 (1954) 775.

[36] Barman, J., Banik, B., and Sultana, F., Romanian J. Biophysics., 31 (2021) 175.

[37] Barman, J., J. Nanostructure., 11 (2021) 661.

[38] Chen, W., Wang, J., and Wang, M.R, Vacuum, 81 (2007) 894.